



Article

Controlling PMSG Wind Turbine Connected to Three Level Neutral Point Clamped Inverter Based on MPC

Mostafa Al-Gabalawy^{1,*}, Ibrahim A. Abdel-Sattar², Mohamed M. M. Salama² and Mohamed M. F. Darwish^{2,*}

¹Department of Electrical Engineering, Faculty of Engineering, Suez University, Suez, Egypt

²Department of Electrical Engineering, Faculty of Engineering at Shoubra, Benha University, Cairo, Egypt

E-mail: mostafagalawy@gmail.com, mohamed.darwish@feng.bu.edu.eg

Received: 16 October 2023; **Revised:** 22 November 2023; **Accepted:** 27 November 2023

Abstract: Wind energy generation systems are facing increasing importance in terms of harmonic distortion control and power quality standards. In recent years, variable speed has also risen rapidly due to advancements in power electronics. The three key elements of a wind power conversion system (WECS) are electrical generators, machine-side converters, and grid-side converters. It should be noted that the permanent magnet synchronous generator is one of the most often used types of electrical generators due to its special qualities. When wind energy is converted to the proper electrical power, it may be injected into the utility grid using either synchronous generators or grid-side converters. Therefore, an investigation of several topologies and control strategies is required to determine which is the best for the machine-side converter. The use of model predictive control (MPC) for a surface mount permanent magnet synchronous machine wind turbine is the main topic of this work. The machine's electrical model is the one that was utilized. The power converters are selected considering the intricate and highly nonlinear aerodynamic system of the wind turbines. MPC is a promising control technique despite being a relatively recent application in power electronics. In addition, MATLAB and Simulink are used to build the MPC code and offer a simplified model of the turbine.

Keywords: WECS, permanent magnet synchronous generator (PMSG), wind turbine, rectifier, inverter, transformer, utility grid, machine-side converter (MSC), grid-side converter (GSC), neutral point clamped (NPC).

1. Introduction

There is a surplus of interest in environmentally friendly and practical forms of energy such as solar power, wind energy, biomass, wave energy, etc. because of the rising energy demand and the rapid depletion of conventional energy sources, which pose a threat to the environment [1,2]. The era of wind turbine power generation began in the 1980s [3]. Wind turbines have grown in size over the last thirty years, with the current maximum capacity per unit [4]. Wind power's rapid incorporation into the electrical grid has raised many concerns about the safety and reliability of the current electric power system. Wind farms, or massive wind turbines, have been connected to the grid in several nations after their grid standards were amended [5]. Power electronic converters have been a staple of the wind energy industry since commercial wind turbines have been operating on the grid. There have been significant advancements in this technology in the last 30 years [6–8].

Among all these energy sources, wind energy is the most attractive because of its efficiency and affordability. With 77.6 GW of additional wind-producing capacity added to the world's energy networks in

2022. Figure 1 presents the results of the most recent analysis of wind generation worldwide with increasing installed wind capacity to 906 GW overall (i.e., a 9% increase over 2021). Note that the top five global markets for new installations were Finland, China, the United States, the United Kingdom, and Sweden. The amount of wind energy produced in 2026 and 2030 will nearly double and increase by 1.8 times, respectively [9–11].

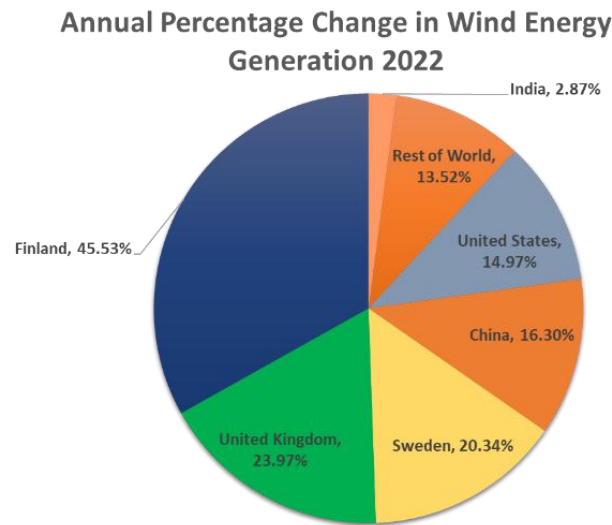


Figure 1. Gigawatts of installation energy.

Furthermore, when looking at the installed capacity annually, the most popular renewable energy source now is wind energy with the quickest growth. In contrast to other alternative sources of energy, the commercial phase of the wind energy business is maturing. Further, wind turbines are constantly growing both in size and nominal generation capacity in order to provide electricity at a more affordable price than from traditional sources [12,13]. Furthermore, to solve the issue of robust multiscale coordination control, ref. [14] has looked at the issue in directed networks against a group of hostile or uncooperative nodes. Additionally, a multiscale filtering technique based on local data that is resistant to both Byzantine and defective nodes has been created. In addition to establishing the necessary and sufficient criteria that provide multiscale consensus with generic time-changing scales in the face of both locally and globally bounded threats, this builds on the idea of network robustness.

MPC is a control method that adjusts and maximizes a control system's inputs in order to minimize expected output error and eventually accomplish the reference control goal. By using this method, the objective function is solved, and an ideal input sequence is found at each sample time (T_s). Following each time step, the plant's present condition is taken into account as the beginning state, and the procedure described above is repeated as in Figure 2.

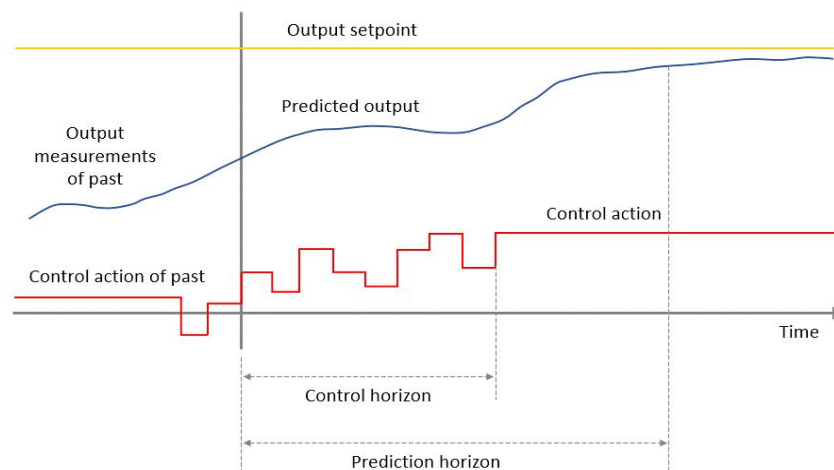


Figure 2. Model predicative control principle of PMSG.

In the previous literature, the primary requirement for wind energy conversion systems (WECSs) to maintain the power generated by the wind turbine at its maximum value while enhancing aerodynamic properties is the modeling of the appropriate blade pitch control scheme [15,16]. The direct-drive permanent magnet synchronous generator (PMSG) has several appealing characteristics, including fewer maintenance requirements, hefty gearbox removal, and increased energy density [17]. The others [18], suggested and proved that a reliable FCSMPC approach with updated forecasts works. In [19] presented a plan for frequency control that may be used with isolated grid wind turbine generators (WTGs). The authors of [20] suggested using a new type of modulated predictive current control that requires less computing power for a three-phase back-to-back linked neutral-point clamped (NPC) converter in a wind energy system that uses permanent magnet synchronous generators (PMSGs). In [21], the amplification of high-frequency noise pollution is addressed by proposing a new hybrid parallel cascaded extended state observer model-free predictive control framework that makes use of a three-level neutral-point-clamped (NPC) power electronic converter. In [22] provides a high-power wind turbine operation plan that complies with the standards of the next-generation grid code and is supported by model predictive control (MPC). More than two voltage levels can be achieved using a three-level Neutral Point Clamped (3L-NPC) back-to-back converter, although far fewer components are needed than, say, five-level topologies [23–27]. Thus, a potential design for high-power wind energy applications is a direct-drive PMSG wind turbine system with a 3L-NPC back-to-back power converter using model predictive control. With the suggested design, the NPC inverter's cost function solely consists of reference monitoring and switching frequency reduction, which improves grid current quality and DC-link capacitor voltage balancing.

A novel power converter topology based on a model prediction technique is presented in this dissertation for wind turbines with three-level ratings. The converter-based variable-speed wind turbines are designed to achieve high-performance operation. Additional benefits of MPC include its dynamic response and flexibility to incorporate irregularities and limitations in controller design. It is therefore a relatively new application of MPC in power electronics, yet it is a promising means of controlling the system. MATLAB and Simulink codes were generated depending on a simplified turbine model. Passive converters at the generator end are combined with multilevel converters at the grid end of the configuration. Furthermore, it includes fewer active switches than BTB-NPC converters, which reduces control system complexity and total cost. As fewer switching states are involved with the recommended topology, computational costs are lower than with BTB-NPC converters. Additionally, linear controllers and modulation stages are eliminated by the MPC approach. The result is a dynamic response that is excellent. NPC inverters also regulate reactive power and the net dc-bus voltage. A noticeable improvement has been made in the quality of the grid power. Based on simulation results using the proposed topology, the voltages on the DC-link capacitors are equally balanced regardless of the reduction in the NPC inverter switching frequency. As the weighting factor changes from 0 to 5000, the NPC inverter switching frequency changes from 1142 to 365 Hz, and the grid current THD increases from 2.63 to 4.82 %. The suggested design only improves grid current quality and DC-link capacitor voltage balancing with reference monitoring and switching frequency reduction, which is the only cost function of the NPC inverter.

2. Mathematics and General Description

A full power rated back-to-back Neutral Point Clamped (NPC). connects the generator to the grid, and when connecting the hub of the wind turbine to the generator shaft, a gearbox is often employed to increase rotational speed. A specialized low-speed multi-pole generator must be employed to provide the necessary nominal frequency in the stator terminals in a direct-drive design, and because the drive train is free of a gearbox, the hub, and rotor may be connected directly.

The produced power is subsequently transferred to the AC grid using back-to-back NPC, which also provides sufficient decoupling due to their DC connection. With this setup, the wind turbine's capacity to tolerate faults is enhanced, and when a grid fault occurs, the generator does not experience harsh transients. The model power converter topology contains a diode rectifier for rectifying the AC voltage to DC first to change the frequency and magnitude of the generator side and integrate the generator side three-phase to the grid side. DC link voltage is connected to a three-level NPC inverter whose configuration can be seen in Figure 3.

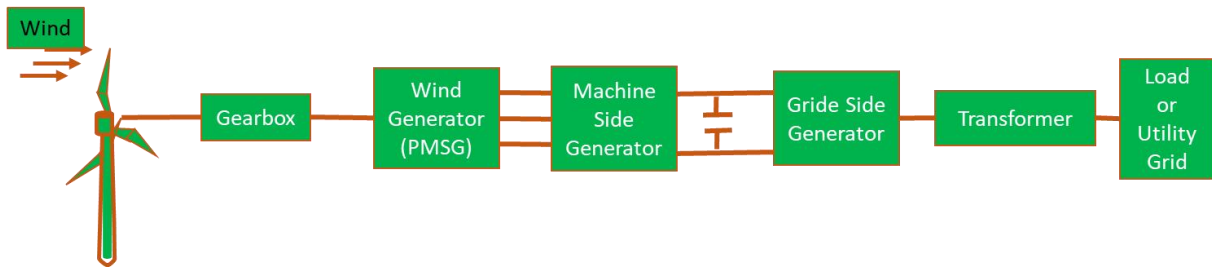


Figure 3. Detailed Circuit Configuration for Grid Side SPMG.

The voltage of the grid side is determined by the switching sequence applied to the generator. From now on, in order to simplify the MPC computations dq frame will be used for current and voltage waveforms. For this abc to dq frame, Park Transformation is used [21] by considering the abc and dq frame illustration, as shown in Figure 4.

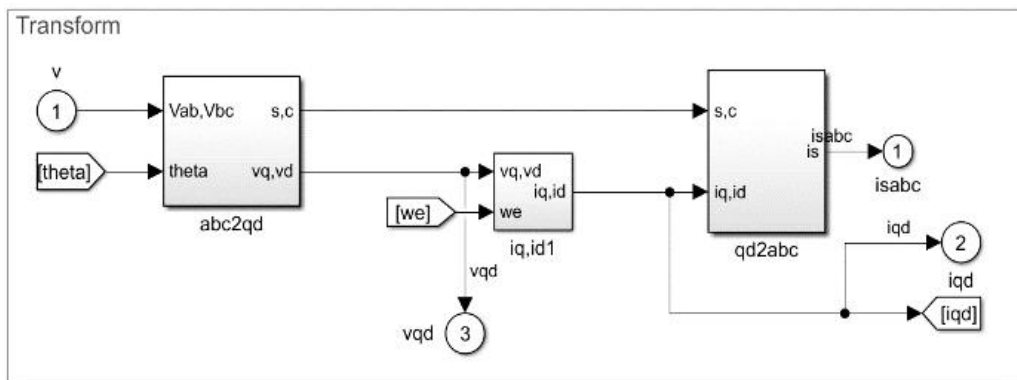


Figure 4. Representation of abc and dq frames of PMSG and angular correspondence.

Hence, the dq voltages will be the inputs of the mathematical model to be built, whereas the dq frame currents will be the state variables. The output to be observed can be selected from anything. However, since the cost function is built to maximize the active power and minimize the reactive power, which is directly related to dq axis currents respectively, the power is selected to be the output to be observed.

The continuous time model for the stator side currents (before the rectifier) is shown in Eq. (1):

$$\frac{d}{dt} \begin{bmatrix} i_{ds} \\ i_{qs} \end{bmatrix} = \begin{bmatrix} -\frac{R_s}{L_{ds}} & \frac{\omega_r L_{qs}}{L_{ds}} \\ \frac{\omega_r L_{ds}}{L_{qs}} & -\frac{R_s}{L_{qs}} \end{bmatrix} \begin{bmatrix} i_{ds} \\ i_{qs} \end{bmatrix} + \begin{bmatrix} \frac{1}{L_{ds}} & 0 \\ 0 & \frac{1}{L_{qs}} \end{bmatrix} \begin{bmatrix} v_{ds} \\ v_{qs} \end{bmatrix} + \begin{bmatrix} 0 \\ -\frac{\omega_r \psi_{ds}}{L_{qs}} \end{bmatrix} \quad (1)$$

Figure 5 displays the block schematic of the MPC scheme for the NPC rectifier. Moreover, to achieve the DC-link neutral-point voltage control's control goal, the estimator subsystem is employed. two capacitors' voltage included in the DC-link measurement. The DC-branch currents are estimated using the grid-side currents and the ideal switching states of the NPC inverter, see Eq. (2). Lagrange extrapolation is used to advance the reference currents to the (k+1) sampling moment.

$$i_{g,dq}^*(k+1) = 2i_{g,dq}^*(k) - i_{g,dq}^*(k-1) \quad (2)$$

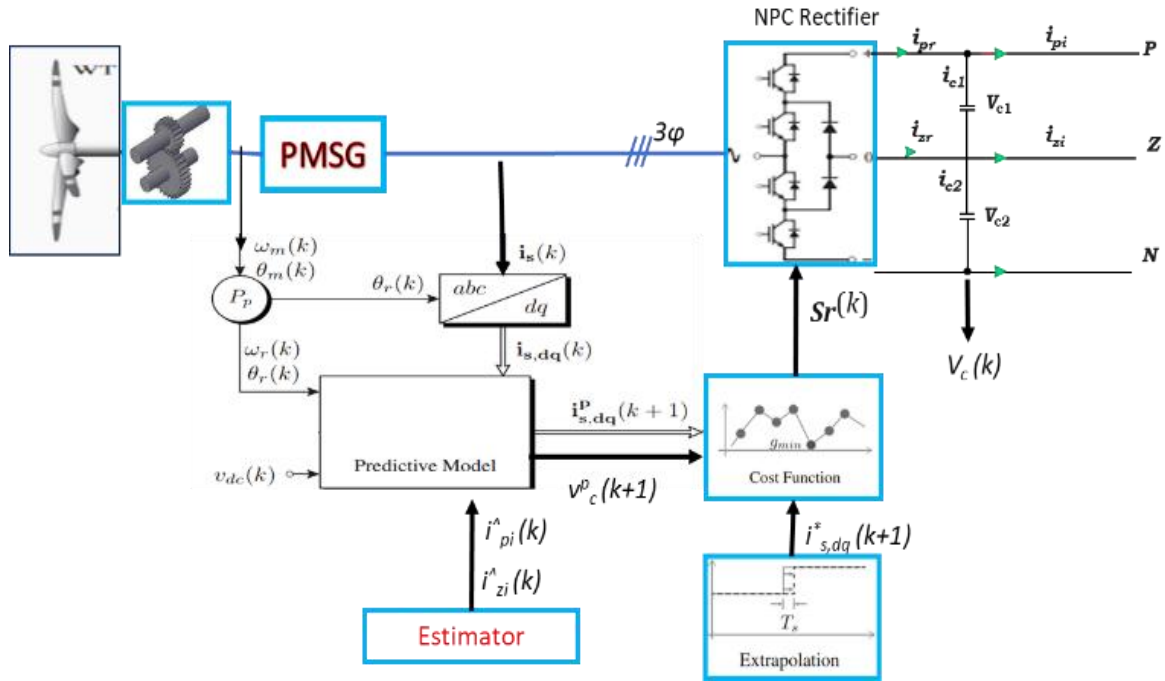


Figure 5. Schematic representation MPC of PMSG side linked with NPC Rectifier.

NPC rectifier terminal voltage predictions are made using the voltage measurements of the DC-link capacitors and the dq-frame switching signals, as in Eq. (3).

$$\begin{bmatrix} v_{ds}^p(k) \\ v_{qs}^p(k) \end{bmatrix} = v_{c1}(k) \begin{bmatrix} S_{dr1}^p(k) \\ S_{qr1}^p(k) \end{bmatrix} + v_{c2}(k) \begin{bmatrix} S_{dr2}^p(k) \\ S_{qr2}^p(k) \end{bmatrix} \quad (3)$$

$$\begin{bmatrix} S_{drj}^p(k) \\ S_{qrj}^p(k) \end{bmatrix} = \begin{bmatrix} T_{\alpha\beta} \\ T_{dq} \end{bmatrix} \begin{bmatrix} S_{arj}^p(k) \\ S_{brj}^p(k) \\ S_{crj}^p(k) \end{bmatrix} \quad (4)$$

$$\begin{bmatrix} i_{ds}^p(k+1) \\ i_{qs}^p(k+1) \end{bmatrix} = \Phi(k) \begin{bmatrix} i_{ds}(k) \\ i_{qs}(k) \end{bmatrix} + \Gamma_w + \Gamma_b \begin{bmatrix} v_{c1}(k) \begin{bmatrix} S_{dr1}^p(k) \\ S_{qr1}^p(k) \end{bmatrix} + v_{c2}(k) \begin{bmatrix} S_{dr2}^p(k) \\ S_{qr2}^p(k) \end{bmatrix} \end{bmatrix} \quad (5)$$

where Φ , Γ_w , and Γ_b represent the DT matrices.

Figure 6 shows the schematic $\alpha\beta$ frame MPC for the linked grid NPC inverter. Starting from measuring the feedback signals grid currents and voltages i_g , v_g , and capacitor voltage v_{c1} . Afterward, the Synchronous Reference Frame Phase Locked Loop (SRF-PLL) method yields the observed grid voltage angle θ_g . So, abc-frame grid transformed into $v_{g\alpha}$ and $i_{g\alpha\beta}$. Then, $\alpha\beta_{ref}$ -axes currents derived from v_{dc}^* and Q_g^* loops were used to implement the MPC strategy with the generator side. For enhancing the transient performance, a 1st order extrapolation is used in Eq. (2).

For a surface mount machine, L_{ds} and L_{qs} are the same. A similar model for the grid side three phase is accurate. Similarly, the grid side discrete-time current representation is shown in Eq. (2).

$$\begin{bmatrix} v_{dg}(k) \\ v_{qg}(k) \end{bmatrix} = v_{c1}(k) \begin{bmatrix} \cos \theta_g(k) & \sin \theta_g(k) \\ -\sin \theta_g(k) & \cos \theta_g(k) \end{bmatrix} \begin{bmatrix} T_{abc} \\ T_{\alpha\beta} \end{bmatrix} \begin{bmatrix} S_{a1l}(k) \\ S_{b1l}(k) \\ S_{c1l}(k) \end{bmatrix} \quad (6)$$

where $v_{dg}(k)$ and $v_{qg}(k)$ represent grid voltages, respectively on the dq-axes. Further, $T_{abc/\alpha\beta}$ represents abc to $\alpha\beta$ frame transformation matrix.

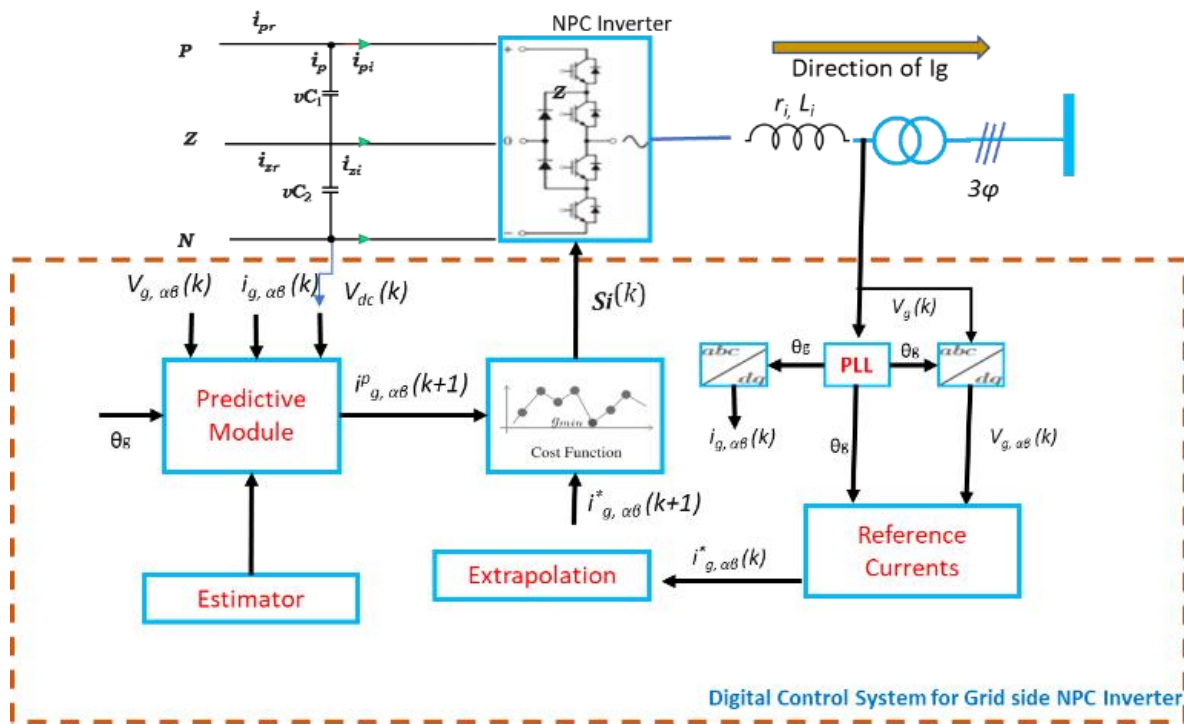


Figure 6. Schematic representation MPC linked with NPC inverter.

For a prediction made one sample in advance, all of these objectives are contained in a quadratic cost function as Eq. (7):

$$G_i(k) = \lambda_{i\alpha} i_{g\alpha}(k) + \lambda_{i\beta} i_{g\beta}(k) + \lambda_{dc} i_{gdc,i}(k) + \lambda_{sw} i_{gsw,i}(k) \quad (7)$$

where $\lambda_{i\alpha}$, $\lambda_{i\beta}$, $\lambda_{dc,i}$ and $\lambda_{sw,i}$ represent the weighting factors for both the d and q axes.

$$\lambda_{i\alpha} = \lambda_{i\beta} = \frac{I_{Bg}}{I_{Bg}^*} = 1, \quad \lambda_{dc,i} = \frac{I_{Bg}}{V_{dc}^*} \quad (8)$$

To determine the best switching state combination that minimizes the cost function, expected i_{ds} and i_{qs} are compared to the current dq-axes reference. Throughout $(k + 1)$ sample time, the NPC receives the specified switching states.

Figure 7 describes the MPC tracking for the reference. By measuring DC voltage, grid current, and voltage, then, calculate currents in the dq-axes grid for the $(k + 1)$ -state. In an iterative loop, the MPC predicts the grid currents and output voltages of the NPC while also minimizing the cost function. Then, choosing an ideal vector and related switching signals, which are subsequently applied straight to the NPC. Then, the extrapolated references are compared with the expected variables at each cycle. During the subsequent sampling period, the switching state (out of 27) that minimizes the cost function is selected and applied to the NPC inverter gating terminals.

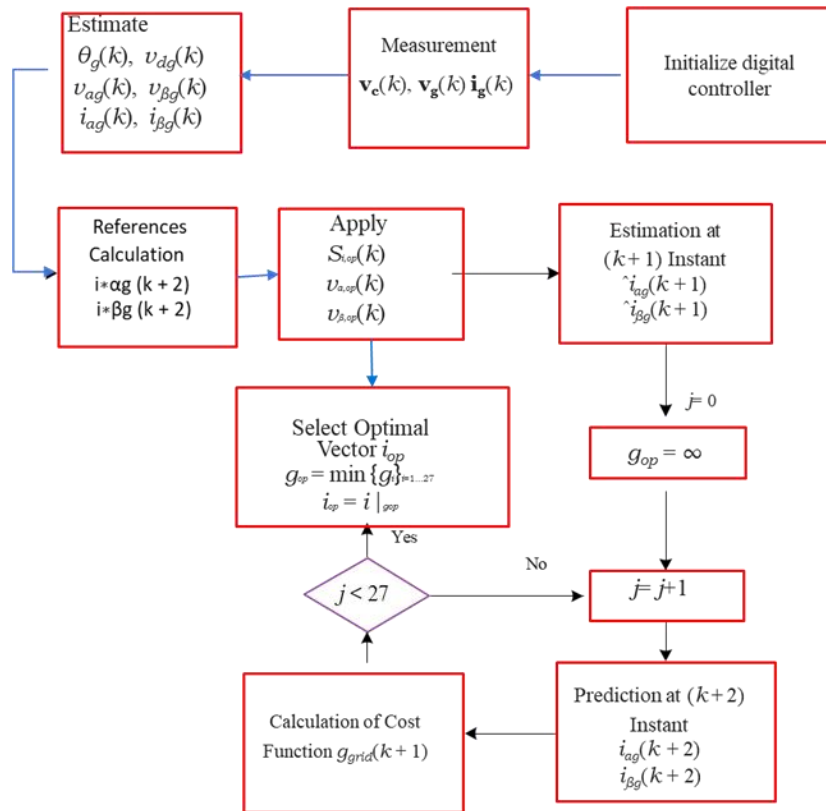


Figure 7. Proposed predictive control algorithm with delay compensation for NPC inverter

3. System Constraints and Parameters

There are several different wind turbine generator types with different power specifications. Using a passive generator side machine, a low-power machine was selected for modelling and its parameters to be used are shown in Table 1.

Table 1. Parameters of the proposed wind energy conversion system

Ps	3.6 MW
Qs	152 kVAR
Vs (Stator phase r.m.s voltage)	1700V
Is (Stator phase r.m.s current)	582 A
fs – ωs (Generator electrical stator frequency)	9.75 Hz
T _m Rated Mechanical Torque (kN.m)	1283 KN.m
R _s Stator Winding Resistance	38.5 mΩ
L _d d-axis Synchronous Inductance	9.75 mH
L _q q-axis Synchronous Inductance	9.75mH
T _s Sampling time	100 μ
λ _{dc,b} Weighting factor	0.1
λ _{sw,b} Weighting factor	100
λ _{sw,i} Weighting factor	100

Therefore, while simulating there will be a constraint on the input voltages not to exceed the rated value provided. Additionally, by using 540 V DC voltage as the passive rectification output, thinking the operation is ideal.

4. MATLAB / SIMULINK Model Predictive Control Implementation

It is proposed to develop a medium voltage (MV) converter for power conversion systems based on permanent magnet synchronous generators (PMSGs) for wind energy. This inverter is made up of a diode rectifier, a three-level boost converter, and a neutral-point clamp (NPC) inverter.

From Figure 8, it is seen how direct-driven PMSG-based WECS convert energy into power. To perform three steps of AC/DC, DC/DC, and DC/AC, a diode rectifier, a Three Level Boost (TLB) converter, and an NPC inverter is utilized. Due to the requirement for a diode rectifier in a WECS, only the generating mode can be used. As a result, the direction of power flow is limited. Grid-tied NPC inverters have two DC-linked capacitors and the TLB's output perfectly matches them. NPC inverters are connected to MV grids via L filters. In comparison to two-level converters, the multilevel and medium voltage operation of NPC improves the power quality and efficiency of the system.

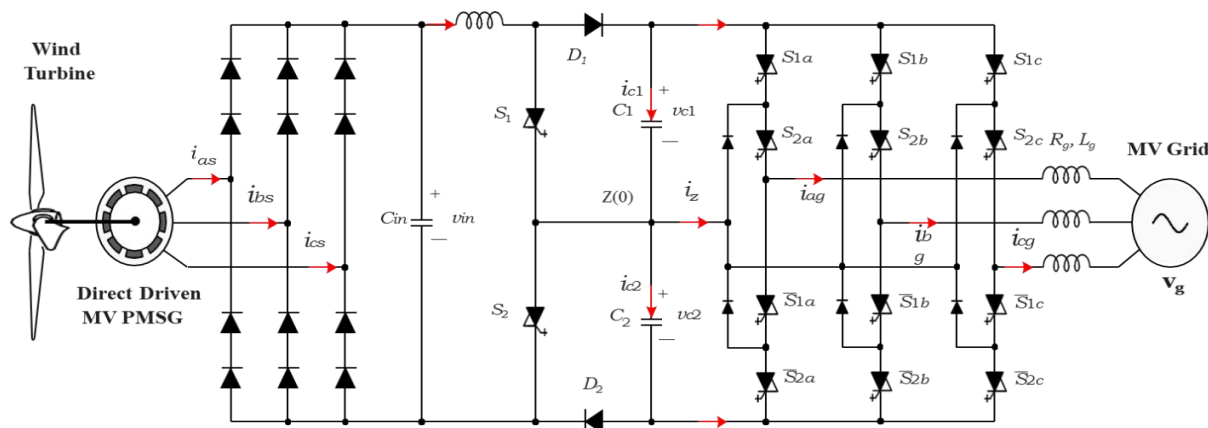


Figure 8. Configuration of medium voltage PMSG-WECS based TLB-NPC converters.

In Figure 9, we show a simplified WECS that can be used for modeling the Three Level Boost converter.

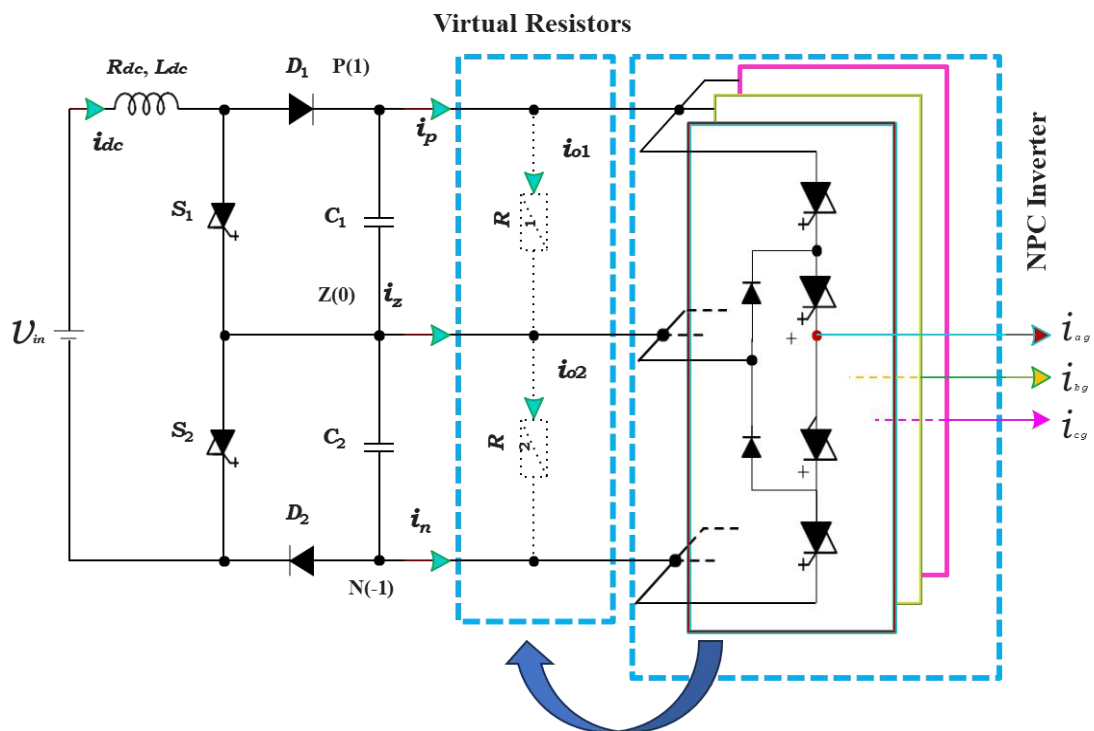


Figure 9. Simple power circuit for the TLB converter step of dc-dc conversion.

The NPC inverter manages the dc-bus voltage and reactive power generation. To demonstrate the effectiveness of the proposed power converters NPC, we present the following model in Figure 10.

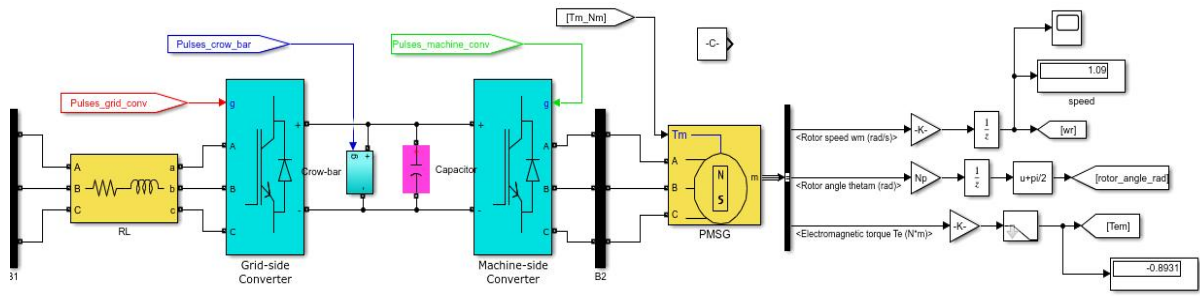
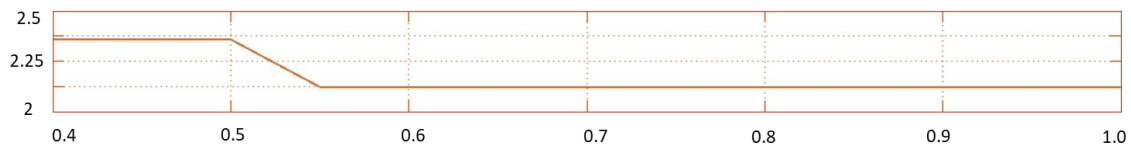


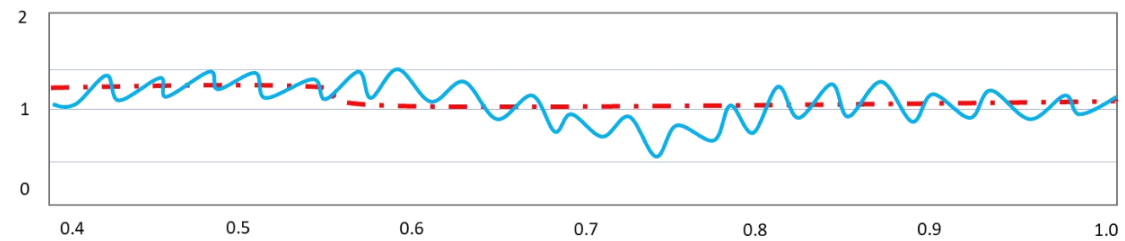
Figure 10. Proposed model predictive control scheme NPC converter based PMSG-WECS.

A power converter's structure and control method are shown in Figures 8 and 9. In Table 1, the WECS values for 3 MW/3000 V/577 A are simulated in MATLAB/Simulink. We assumed that the PMSG used surface mount magnets and the one-step prediction horizon was $L_d = L_q$.

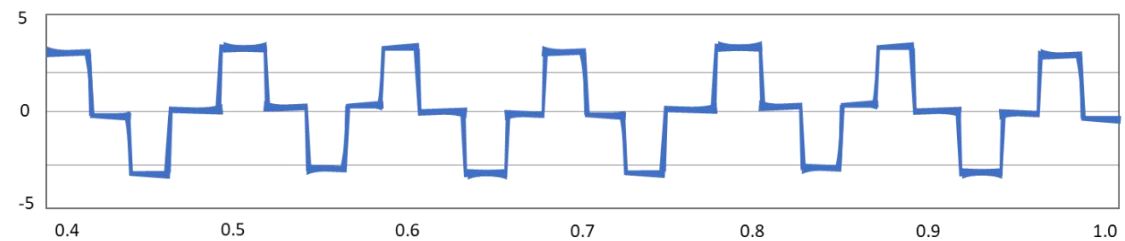
It is estimated that the wind speed (3 p.u.) is 15 m/s when the generator is initially running at its rated speed. PMSG stator voltage and current waveforms are distorted due to diode switching, and electromagnetic torque, T_e , is achieved by three-phase currents in the generator that have harmonics. Boost converters maintain dc-link current and i_{dc} 's reference values, while grid-side inverters regulate reactive power and net DC-bus voltage. With a total harmonic distortion (THD) of 2.76 percent, the phase angle between grid voltage and current is zero. The grid current, however, is 560 A. There are 2.91 MVARs of apparent power and 2.91 MWs of active power. There is a significant difference between the 3.6 MW mechanical input power and the generator's rated output. As a result of these operating conditions, NPC inverters have a switching frequency of 900 Hz. Figure 11 shows simulated waveforms with various wind speeds and reactive power references.



(a) PMSG speed, ω_m (rad/s)



(b) T_e and its reference T^* , (MN.m)



(c) line-line voltage, $V_{s,ab}$ (kV)

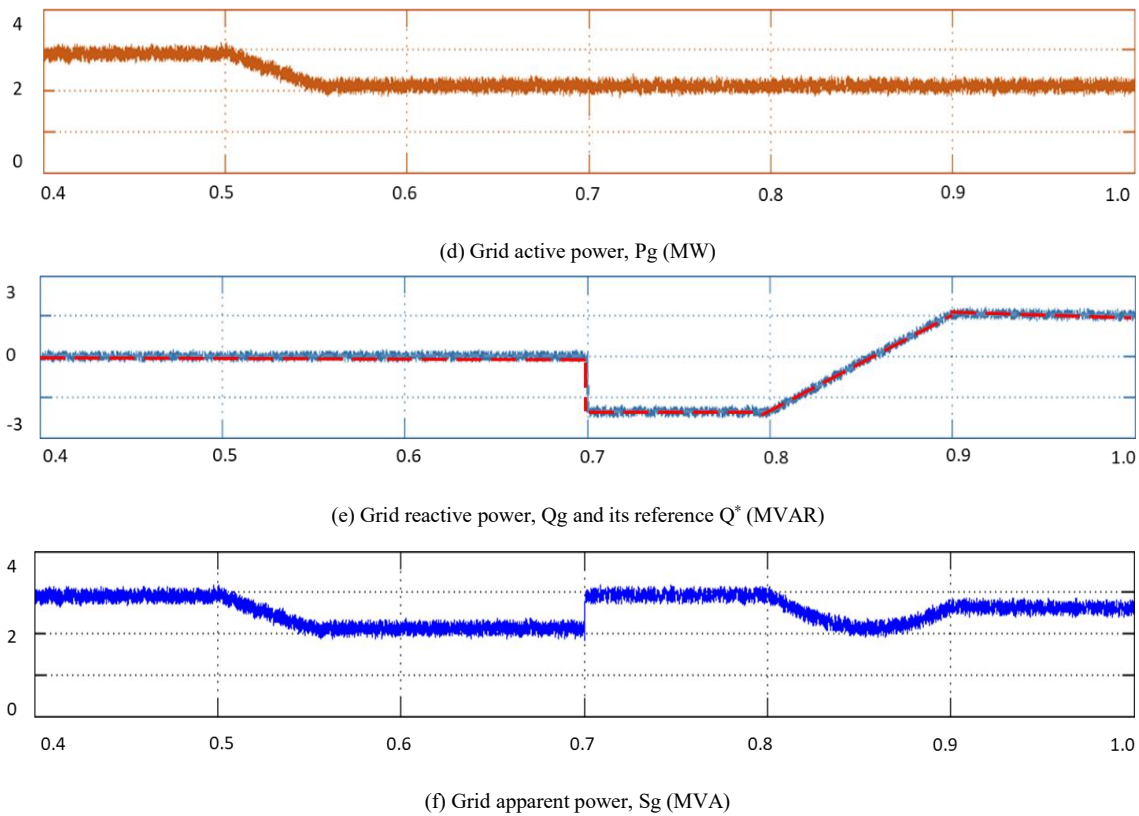


Figure 11. Results of the simulation with a step change in wind speed.

At time $t = 0.5$ s, the wind speed changes steadily from 15 m/s (1 p.u.) to 10.8 m/s (0.9 p.u.). After a short period of transients, the generator speed, generator current, electromagnetic torque, and boost converter input voltage settle to a new value. As a result of the generator speed variations, the MPPT algorithm created a new reference for the DC-link current. By following its reference, the controller acquired MPPT in situations of variable wind speed by making the DC-link current follow its reference. When the wind speed is reduced, grid currents of 409 A with 3.61 % THD change, which affects active power supplied to the grid of 2.13 MW. As for NPC inverters, the switching frequency is 890 Hz. An increase in grid current and reactive power waveforms is applied at $t = 0.7$ s, going from 0 to -2.055 MVAR (-0.685 p.u.). This shows that the grid current and reactive power waveforms respond satisfactorily to the transient condition.

5. Conclusions

The paper describes how to use the simulated technique (MPC) to regulate the entire wind energy system using NPCs in a PMSG-based wind energy system. PMSG properties are measured using a suggested approach. The discrete-time model of the system is used to develop two distinct control loops that minimize cost functions to produce the gating signals to the NPC inverter. Multilevel generator-side converters are combined with passive generator-side converters in the proposed configuration. As a result of the smaller number of active switches required than BTB-NPC converters, the total cost and complexity of the control system are lower as well. With the recommended topology, there are fewer switching states, meaning the computational cost is lower compared to BTB-NPC converters. As well as eliminating linear controllers and modulation stages, the proposed MPC approach eliminates the need for linear controllers. Consequently, it produces an excellent dynamic response. Furthermore, reactive power and voltage are regulated by the NPC inverter. There has been a noticeable improvement in the quality of grid power. Having NPC inverters control independent of the grid has significantly improved power quality. As a final result of the simulations, it is observed that the DC-link

capacitor voltages are perfectly balanced, irrespective of the reduction in NPC inverter switching frequency. Changing the weighting factor from 0 to 5000 reduces the switching frequency of the NPC inverter from 1142 to 365 Hz and increases the grid current THD from 2.63 to 4.82 %. This design solely benefits grid current quality and DC-link capacitor voltage balancing by reducing switching frequency and monitoring reference values.

Conflict of Interest

There is no conflict of interest for this study.

References

- [1] Sarwar, M.; Siddiqui, A.S.; Ghoneim, S.S.M.; Mahmoud, K.; Darwish, M.M.F. Effective Transmission Congestion Management via Optimal DG Capacity Using Hybrid Swarm Optimization for Contemporary Power System Operations. *IEEE Access* **2022**, *10*, 71091–71106, <https://doi.org/10.1109/access.2022.3187723>.
- [2] Ibrahim, N. F.; Mahmoud, k.; Lehtonen, M.; Darwish, M. M. F. Comparative Analysis of Three-Phase PV Grid Connected Inverter Current Control Schemes in Unbalanced Grid Conditions. *IEEE Access* **2023**, *11*, 42204–42221, <https://doi.org/10.1109/access.2023.3270262>.
- [3] Petrović, V.; Jelavić, M.; Baotić, M. MPC framework for constrained wind turbine individual pitch control. *Wind Energy* **2021**, *24*, 54–68, <https://doi.org/10.1002/we.2558>.
- [4] Ali, M.N.; Soliman, M.; Mahmoud, K.; Guerrero, J.M.; Lehtonen, M.; Darwish, M.M.F. Resilient Design of Robust Multi-Objectives PID Controllers for Automatic Voltage Regulators: D-Decomposition Approach. *IEEE Access* **2021**, *9*, 106589–106605, <https://doi.org/10.1109/access.2021.3100415>.
- [5] Abubakr, H.; Vasquez, J.C.; Mahmoud, K.; Darwish, M.M.; Guerrero, J.M. Comprehensive review on renewable energy sources in Egypt—current status, grid codes and future vision. *IEEE Access* **2022**, *10*, 4081–4101, <https://doi.org/10.1109/ACCESS.2022.3140385>.
- [6] Al-Gabalawy, M.; Hosny, N.S.; Hussien, S.A. Cuckoo search algorithm based for tuning both PI and FOPID controllers for the DFIG-Wind energy conversion system. *Int. J. Electr. Comput. Eng.* **2020**, *10*, 6319–6329, <https://doi.org/10.11591/ijece.v10i6.pp6319-6329>.
- [7] Al-Gabalawy, M.; Ramadan, H.S.; Mostafa, M.A.; Hussien, S.A. Power Curve Estimation of a Wind Turbine Considering Different Weather Conditions using Machine Learning Algorithms. In Proceedings of 2022 23rd International Middle East Power Systems Conference (MEPCON), Cairo, Egypt, 13–15 December **2022**, <https://doi.org/10.1109/MEPCON55441.2022.10021759>.
- [8] Chaudhuri, A.; Datta, R.; Kumar, M.P.; Davim, J.P.; Pramanik, S. Energy conversion strategies for wind energy system: Electrical, mechanical and material aspects. *Materials* **2022**, *15*, 1232, <https://doi.org/10.3390/ma15031232>.
- [9] Al-Gabalawy, M.; Salama, M.M.; Abdel-Sattar, I.A.; Darwish, M.M. Intelligent Control for Wind Turbines Connected to Utility Grid using MPC. In Proceedings of 2022 23rd International Middle East Power Systems Conference (MEPCON), Cairo, Egypt, 13–15 December **2022**, <https://doi.org/10.1109/MEPCON55441.2022.10021734>.
- [10] Liu, X.; Feng, L.; Kong, X. A Comparative Study of Robust MPC and Stochastic MPC of Wind Power Generation System. *Energies* **2022**, *15*, 4814, <https://doi.org/10.3390/en15134814>.
- [11] Al-Gabalawy, M.; Mahmoud, K.; Darwish, M.; Dawson, J.; Lehtonen, M.; Hosny, N. Reliable and Robust Observer for Simultaneously Estimating State-of-Charge and State-of-Health of LiFePO₄ Batteries. *Appl. Sci.* **2021**, *11*, 3609, [doi:10.3390/app11083609](https://doi.org/10.3390/app11083609).
- [12] Lin, Z.; Chen, Z.; Liu, J.; Wu, Q. Coordinated mechanical loads and power optimization of wind energy conversion systems with variable-weight model predictive control strategy. *Appl. Energy* **2018**, *236*, 307–317, <https://doi.org/10.1016/j.apenergy.2018.11.089>.
- [13] Badger, M.; Zuo, H.; Hannesdóttir, A.; Owda, A.; Hasager, C. Lifetime prediction of turbine blades using global precipitation products from satellites. *Wind. Energy Sci.* **2022**, *7*, 2497–2512, <https://doi.org/10.5194/wes-7-2497-2022>.
- [14] Shang, Y. Resilient Multiscale Coordination Control against Adversarial Nodes. *Energies* **2018**, *11*, 1844, <https://doi.org/10.3390/en11071844>.

- [15] Wang, H.; Yang, J.; Chen, Z.; Ge, W.; Ma, Y.; Xing, Z.; Yang, L. Model Predictive Control of PMSG-Based Wind Turbines for Frequency Regulation in an Isolated Grid. *IEEE Trans. Ind. Appl.* **2018**, *54*, 3077–3089, <https://doi.org/10.1109/tia.2018.2817619>.
- [16] Zhang, A.; Yaramasu, V.; Rodriguez, J.; Zhang, Z. Modulated Predictive Current Control of Back-to-Back NPC Converter in PMSG Wind Energy System with Reduced Computational Burden. In Proceedings of 2022 IEEE 7th Southern Power Electronics Conference (SPEC), Nadi, Fiji, 5–8 December **2022**, <https://doi.org/10.1109/SPEC55080.2022.10058345>.
- [17] Mayilsamy, G.; Lee, S.R.; Joo, Y.H. An improved model predictive control of back-to-back three-level NPC converters with virtual space vectors for high power PMSG-based wind energy conversion systems. *ISA Trans.* **2023**, <https://doi.org/10.1016/j.isatra.2023.09.033>.
- [18] Li, J.; Zhang, Z.; Yang, X. A novel model predictive control strategy of D-PMSG wind turbine systems for LVRT based on two-state unloading resistance and super capacitor. *J. Physics: Conf. Ser.* **2023**, *2418*, 012048, <https://doi.org/10.1088/1742-6596/2418/1/012048>.
- [19] Saberi, S.; Rezaie, B. Computationally efficient direct predictive speed control of PMSMs fed by three-level NPC converters with guaranteed stability. *J. Power Electron.* **2022**, *22*, 1131–1141, <https://doi.org/10.1007/s43236-022-00437-7>.
- [20] Li, J.; Babayomi, O.; Zhang, Z.; Li, Z. Robust Predictive Current Control of PMSG Wind Turbines with Sensor Noise Suppression. *Energies* **2023**, *16*, 6255, <https://doi.org/10.3390/en16176255>.
- [21] Catalán, P.; Wang, Y.; Chen, Z.; Arza, J. Model Predictive Control-enabled Fault Ride Through Operation Strategy for High Power Wind Turbine. In Proceedings of 2022 24th European Conference on Power Electronics and Applications (EPE'22 ECCE Europe), Hanover, Germany, 5–9 September **2022**.
- [22] Xie, H.; Tian, W.; Gao, X.; Wang, F.; Rodríguez, J.; Kennel, R. An Ensemble Regulation Principle for Multiobjective Finite-Control-Set Model-Predictive Control of Induction Machine Drives. *IEEE Trans. Power Electron.* **2023**, *38*, 3069–3083, <https://doi.org/10.1109/TPEL.2022.3220289>.
- [23] Ke, D.; Wang, F.; He, L.; Li, Z. Predictive Current Control for PMSM Systems Using Extended Sliding Mode Observer with Hurwitz-Based Power Reaching Law. *IEEE Trans. Power Electron.* **2020**, *36*, 7223–7232, <https://doi.org/10.1109/tpel.2020.3043489>.
- [24] Prince, M.K.K.; Arif, M.T.; Gargoom, A.; Oo, A.M.T.; Haque, E. Modeling, Parameter Measurement, and Control of PMSG-based Grid-connected Wind Energy Conversion System. *J. Mod. Power Syst. Clean Energy* **2021**, *9*, 1054–1065, <https://doi.org/10.35833/mpce.2020.000601>.
- [25] Gajewski, P.; Pieńkowski, K. Control of wind turbine system with PMSG for low voltage ride through. In Proceedings of the International Symposium on Electrical Machines, Andrychow, Poland, 10–13 June **2018**, <https://doi.org/10.1109/ISEM.2018.8442464>.
- [26] Mousa, H.H.; Youssef, A.R.; Mohamed, E.E. Model predictive speed control of five-phase PMSG based variable speed wind generation system. In Proceedings of 2018 Twentieth International Middle East Power Systems Conference (MEPCON), Cairo, Egypt, 18–20 December **2018**, <https://doi.org/10.1109/MEPCON.2018.8635190>.
- [27] Elsis, M.; Mahmoud, K.; Lehtonen, M.; Darwish, M.M.F. Effective Nonlinear Model Predictive Control Scheme Tuned by Improved NN for Robotic Manipulators. *IEEE Access* **2021**, *9*, 64278–64290, <https://doi.org/10.1109/access.2021.3075581>.